

## STRUCTURAL, MORPHOLOGICAL AND DISSOLUTION PROPERTIES OF ZrO<sub>2</sub>-BASED BIOCOMPOSITES FOR DENTAL APPLICATIONS

LILIANA BIZO<sup>a</sup>, KLARA SABO<sup>a</sup>, RÉKA BARÁBAS<sup>b</sup>,  
GABRIEL KATONA<sup>b</sup>, LUCIAN BARBU-TUDORAN<sup>c,d</sup>,  
ANTONELA BERAR<sup>e,\*</sup>

**ABSTRACT.** In the present work, zirconia-based biocomposites were prepared by adding different amounts of antibacterial magnesium oxide and bioactive and biocompatible hydroxyapatite (HAP). The biocomposites were synthesized by the conventional ceramic processing route. The structure and morphology of the materials were investigated using X-ray powder diffraction (XRPD), scanning and transmission electronic microscopy (SEM and TEM). The stability of the tetragonal structure of ZrO<sub>2</sub> was confirmed by XRPD analyses. Moreover, their bioactivity was studied by soaking the samples in artificial saliva (AS) to evaluate the effect of MgO and HAP on the biological performances of the prepared biocomposites. UV-VIS analyses carried out on artificial saliva after immersion of the prepared materials showed that MgO plays an important role in the post-immersion dissolution process.

**Keywords:** zirconia (ZrO<sub>2</sub>), magnesium oxide (MgO), hydroxyapatite (HAP), biocomposites.

---

<sup>a</sup> Babeş-Bolyai University, Faculty of Chemistry and Chemical Engineering, Department of Chemical Engineering, 11 Arany Janos str., RO-400028, Cluj-Napoca, Romania

<sup>b</sup> Babeş-Bolyai University, Faculty of Chemistry and Chemical Engineering, Department of Chemistry and Chemical Engineering of Hungarian Line of Study, 11 Arany Janos str., RO-400028, Cluj-Napoca, Romania

<sup>c</sup> Babeş-Bolyai University, Faculty of Biology and Geology, Department of Molecular Biology and Biotechnology, 1 Mihail Kogălniceanu str., RO-400084, Cluj-Napoca, RO-400015, Romania

<sup>d</sup> National Institute for Research and Development of Isotopic and Molecular Technologies, 67-103 Donath Street, RO-400293, Cluj-Napoca, Romania

<sup>e</sup> "Iuliu Hațieganu" University of Medicine and Pharmacy, Faculty of Dentistry, Department of Prosthetic Dentistry and Dental Materials, 32 Clinicilor str., RO-400006, Cluj-Napoca, Romania

\* Corresponding author: [berar.antonela@umfcluj.ro](mailto:berar.antonela@umfcluj.ro)

## INTRODUCTION

Beside many dental ceramic materials, zirconia ( $ZrO_2$ ) has been considered to be of great importance, due to its exceptional physical and biological properties and many researches were published on the synthesis of zirconia-based dental materials for applications in dental implants and prostheses [1-11].  $ZrO_2$  is an oxide which presents three types of crystalline structures at ambient pressure as follow: the monoclinic phase ( $m-ZrO_2$ ), which is stable from room temperature up to 1170 °C and exhibits poor mechanical properties, the tetragonal phase ( $t-ZrO_2$ ), which is stable in the temperature range 1170–2370 °C and has good mechanical properties, and the cubic phase ( $c-ZrO_2$ ), which is stable above 2370 °C and has moderate mechanical properties [12-15]. The spontaneous transformation from the  $t$ -phase to the more stable  $m$ -phase is associated with a volume increase of 3% to 5%. The tension which occurs inside of the different restorations made of pure  $ZrO_2$ , during the cooling after sintering, results in numerous microcracks, which could lead to premature failure of the restoration [16]. In order to stabilize the  $t$ -phase at room temperature, zirconia can be mixed with other metallic oxides, e.g. MgO,  $CeO_2$ ,  $La_2O_3$ , CaO,  $Y_2O_3$ , etc. [17-19]. Yttria-doped tetragonal zirconia polycrystal (Y-TZP) has been the most attractive material in terms of toughness and structural properties and has recently been used for prosthetic rehabilitations as restorative materials in the fabrication of single crowns or fixed partial dentures and also in dental implantology. However, leaching of yttria in humid environments and the related degradation in properties have been a major bottleneck for wider applications of Y-TZP. Conversely, it was demonstrated that magnesium stabilized zirconia has several advantages and can be developed with a good combination of mechanical and tribological properties by using the appropriate preparation technique [20]. Moreover, the advantages of MgO as antibacterial material are multiple, as this oxide is an ample raw material, low cost and safe to human beings. [21]. Its mild antibacterial property lies mainly in the basicity and oxygen vacancies of MgO nanopowders [21-23].

Hydroxyapatite (HAP), a calcium phosphate (CaP) bioceramics similar to the human hard tissues in morphology and composition showed good osteoconductivity and bone-bonding ability [24]. Due to its outstanding properties like bioactivity, biocompatibility, non-toxicity, and non-inflammatory nature, HAP attracted great interest as a biomaterial used in different medical applications among orthopedic and dental implant coating, maxillofacial and dental surgery and restoration of periodontal defects, biodegradable scaffolds, and drug delivery systems occupy an important place.

ZrO<sub>2</sub>-HAP composites are considered to be interesting materials, due to the combination between two bioceramics, the inert ZrO<sub>2</sub> and the active HAP, which could increase the bonding ability with natural bone in many medical fields. For these reasons, in the past decade, many ZrO<sub>2</sub>-HAP composites have been developed as coating or substrate in order to achieve both bone reconstruction and regeneration needed in the treatment of large bone defects [25].

The present work aimed to prepare ZrO<sub>2</sub>-based biocomposites by using different amounts of antibacterial MgO and bioactive and biocompatible HAP, by ceramic method followed by sintering at high temperature. The obtained biocomposites were further analyzed by X-ray powder diffraction (XRD), scanning electron microscopy (SEM) and transmission electron microscopy (TEM). Moreover, UV-VIS spectroscopy was employed to evaluate the bioactivity and biocompatibility of the prepared composites by *in vitro* preliminary tests, after immersion in artificial saliva (AS).

## RESULTS AND DISCUSSION

### Structural Studies

Structural analyses of the prepared composites were performed by XRPD before and after immersion in AS during 32 days. Figure 1 displays the XRPD patterns of biocomposites following sintering in the air at 1550 °C and before immersion in AS. XRPD analysis of powder samples showed that all patterns display a pure tetragonal phase (S.G. P4<sub>2</sub>/nmc,) with peaks at 30.5°, 40.3°, 47.1°, 53.1°, 68.5°, 72.9° and 78.4° corresponding to the (111), (112), (202), (221), (113), (132), (004) and (114) planes of *t*-ZrO<sub>2</sub> (JCPDS card no. 89-7710). By increasing the amount of MgO in the prepared composites, supplementary phase with peaks at 42.98° and 62.49° corresponding to (200) and (220) planes of periclase (MgO) appears, increasing in intensity, as visible from Figure 1. However, no characteristic peaks corresponding to any CaP-compounds, like HAP, TCP (tricalcium phosphate) or TTCP (tetracalcium phosphate) or CaO and CaZrO<sub>3</sub> was detected for any of the samples, within the detection limit of XRPD. These crystal structure transformations are the reactions that generally occur when sintering ZrO<sub>2</sub> and HAP at a high temperature.

The XRPD patterns after immersion in AS are presented in Figure 2. Examination of XRPD patterns indicates structural stability of the tetragonal phase but always accompanied by the periclase phase, with increasing its amount in the prepared biocomposites. As visible from XRPD patterns for S2 sample, pre- and post-immersion, two small peaks at  $2\theta = 28.3^\circ$  and  $31.43^\circ$  belong to (-111) and (111) planes of *m*-ZrO<sub>2</sub> phase, respectively (Figure 1 and Figure 2).

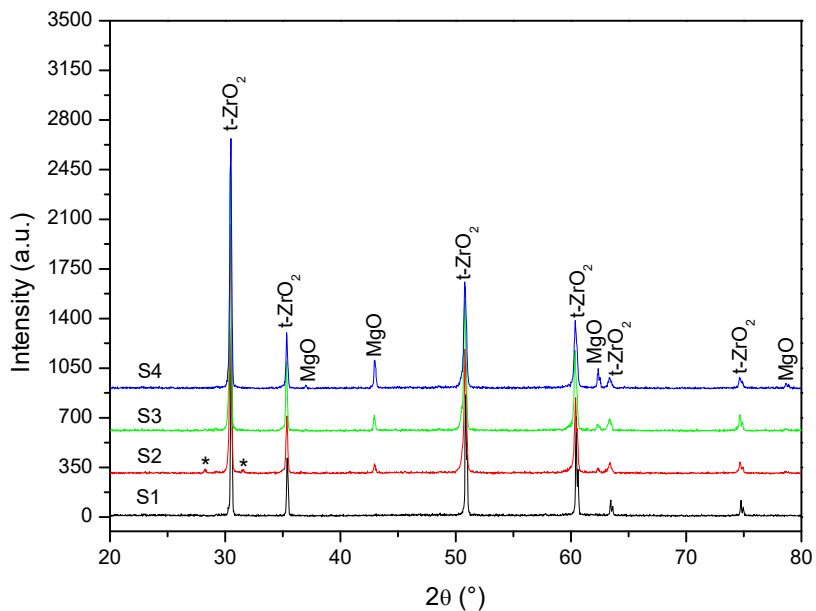


**Figure 1.** XRPD pattern of samples before immersion in AS.

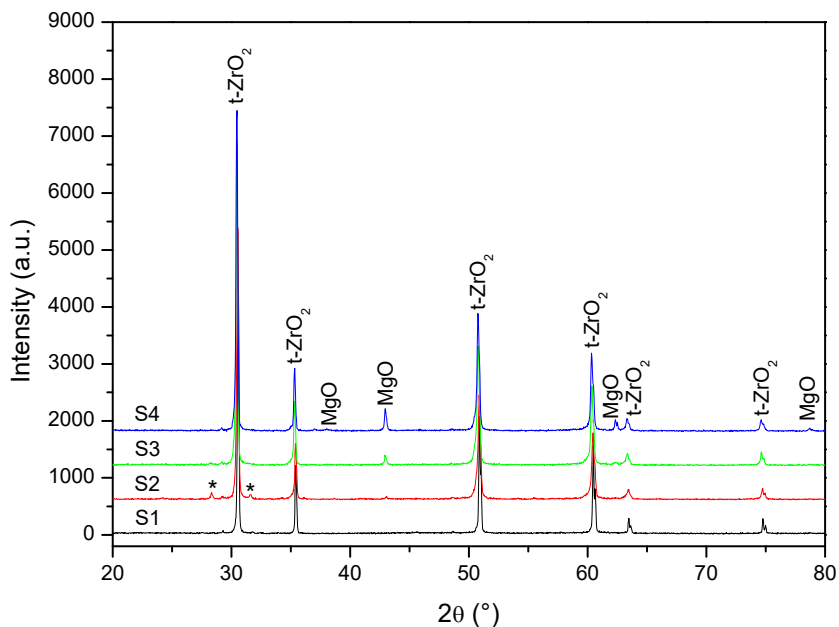


**Figure 2.** XRPD pattern of samples after immersion in AS.

The crystallite sizes (D) of the composites were calculated based upon on the (101) diffraction peak's broadening in the XRD pattern using the Scherrer equation:

$$D_{hkl}=0.9\lambda/(\beta\cos\theta)$$

where: D - crystallite size along (hkl) direction,  $\beta$  - full width half maximum (FWHM) of the most intense diffraction line,  $\lambda$  - wavelength of X-ray,  $\theta$  - the Bragg angle [26].

The evolution of the crystallite sizes in the prepared composites pre- and post-immersion is summarized in Table 1. As listed in Table 1, the crystallite sizes estimated using the Scherrer equation are ranged in the nanometric domain, between 51.91 nm to 71.27 nm. The results suggest the stabilization of ZrO<sub>2</sub> in the tetragonal phase for all the studied composites, which could be attributed to substitution of Zr<sup>4+</sup> by Mg<sup>2+</sup>. Due to their ionic radii, Mg<sup>2+</sup> (0.64 Å) should replace Zr<sup>4+</sup> (0.89 Å) in the normal sites of the lattice, but replacing the host cation with a foreign cation of different radius and valence state introduces strain. The appropriate position for Mg<sup>2+</sup> in the ZrO<sub>2</sub> was Zr<sup>4+</sup> site and the charge difference was compensated by oxygen vacancies [27]. Consequently, substituting the Zr<sup>4+</sup> with a smaller ion, in this case Mg<sup>2+</sup>, leads to a contraction of the lattice.

**Table 1.** Calculated crystallite sizes of composites pre- and post-immersion in AS.

Composition	D <sub>Scherrer</sub> (nm) pre-immersion	D <sub>Scherrer</sub> (nm) post-immersion
S1	71.27	67.03
S2	56.11	51.91
S3	55.56	54.11
S4	52.13	57.68

We can conclude that the weak changes noticed in the XRPD patterns prove that the structural units involved in matrix network are quite stable in the AS environment. However, low intensity peaks corresponding to *m*-ZrO<sub>2</sub>, are presents only on post-immersed S2 sample and could be attributed to the martensitic transformation of *t*-ZrO<sub>2</sub> to *m*-ZrO<sub>2</sub> during cooling.

### Morphological Studies

The morphology of the composites after immersion in AS was examined by SEM and TEM. Figure 3 shows the morphological details of composites and coral-like interconnection of grains in the sintered ceramics. Figure 3a shows the typical connectivity of grains from which the sintering neck can be easily

observed. Between interconnected grains, uniform 2D rectangular MgO micro-sheets stacked in 3D are observed (Figure 3b-d). These MgO micro-sheets have tiny thickness and irregular shape. This type of interconnected structure in zirconia-based materials was previously observed by Hu et al. for yttria-stabilized zirconia ( $ZrO_2$ -8 mol%  $Y_2O_3$ , YSZ) ceramics sintered at 1550 °C [28]. They showed that the strong network provided by the interconnection of grains made it possible for the bodies to obtain high mechanical strength, easy to handle during the fabrication process and more adaptive to the working condition [28].

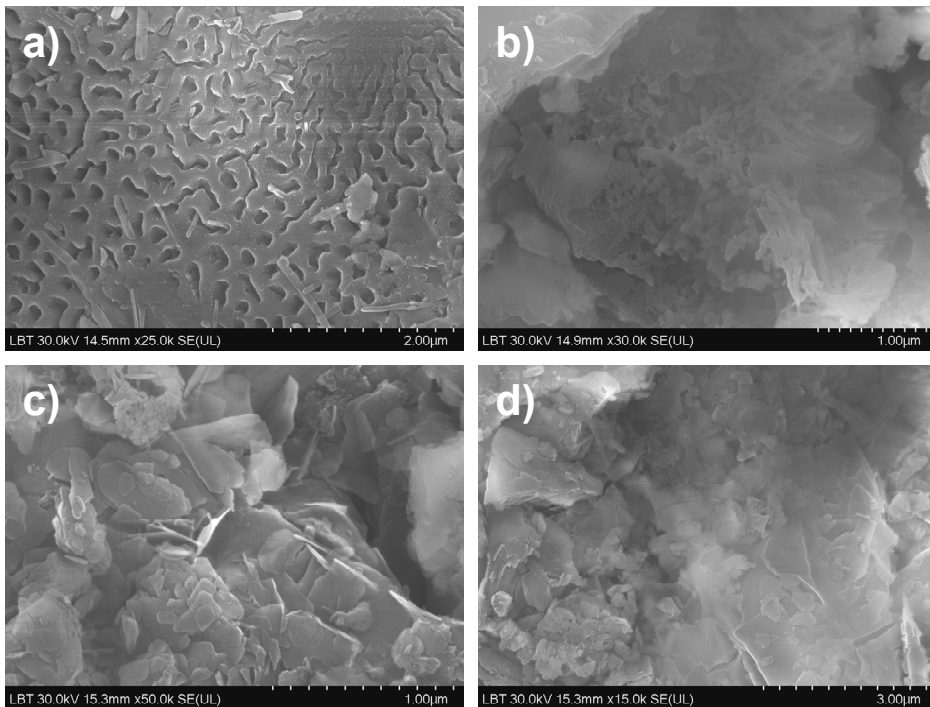


**Figure 3.** SEM images of (a) S1, (b) S2, (c) S3 and (d) S4 biocomposites after immersion in AS.

On the other hand, the microstructural observations reveal the presence of pores as seen in Figure 3a. The presence of such finer pores could favor the initial osteoblast cell attachment by a mechanical anchorage process, even though for an effective osteointegration process large pore sizes are desirable. Once cells are attached at the initial stage of implantation, the attached cell assembly would subsequently favor formation of multiple cells and thereby lead to *in vivo* tissue formation [20, 29]. Therefore, finer pores and less volume

fraction of porosity, as observed in the composites investigated here, should be beneficial from the point of view of both physical properties and biological cell attachment.

TEM images (Figure 4a-d) reveals highly agglomerated particles with size varying in the nanometric domain. These observations are in agreement with the results obtained by XRPD. Although all of the composites produced from the powders consist of fine grains of the ZrO<sub>2</sub>, MgO and HAP phases, these are clustered into coarse-phase domains that are distributed rather inhomogeneously.

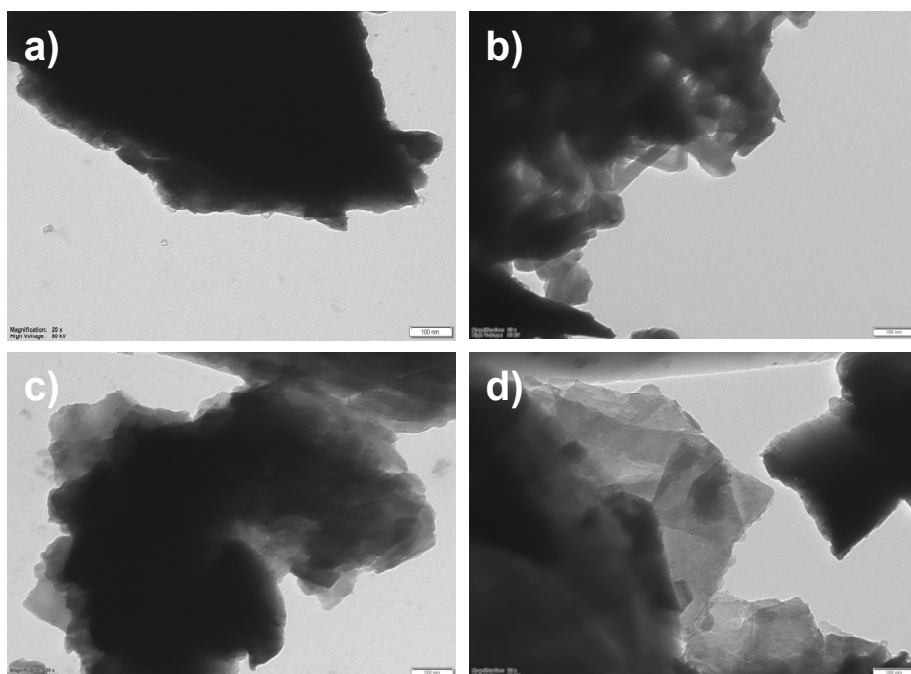


**Figure 4.** TEM images with a 20x magnification (scale bar 100 nm) of (a) S1, (b) S2, (c) S3 and (d) S4 biocomposites after immersion in AS.

### ***In vitro* dissolution analysis**

Figure 5 presents the UV-Vis absorption spectra for the as-prepared AS (AS before composites immersion) and AS after a 32 day immersion time of different prepared composites, further refer to AS1, AS2, AS3 and AS4, which corresponds to AS after immersion of S1, S2, S3, and S4 composites, respectively.

Absorption bands appear at 224 nm and 270 nm in the case of as-prepared AS. As seen from Figure 5, in the case of AS after immersion of composites, an absorption band appears at 205 nm, which is not evidenced in the as-prepared AS. These observed changes could be caused by the migration of ions between the biocomposites and the AS in which it is immersed. As zirconia has chemical stability under physiological conditions, MgO could have a significant impact on the interactions between the composites and AS in which incubation takes place. Due to the relatively weak ionic divalent metal-oxygen bonds, MgO dissolution could proceed by breaking these bonds, which release the  $Mg^{2+}$  ions directly into the solution. The fast dissolution of magnesia contrasts with the behavior of other multi-oxide phases that require the breaking of more than one type of metal-oxygen bond. In these cases, the dissolution mechanism involves the sequential breaking of the bonds, which follows an order according to their reactivity. Taking into account the result obtained by Grima et al. [30] the phenomena which take place can be explained as follow. MgO dissolution is controlled by chemical reactions that involve the dissolution of MgO in a liquid medium to produce  $Mg^{2+}$  and  $OH^-$ . Forwards, due to the water molecules, an intermediate brucite product could be generated and subsequently dissociated into  $Mg^{2+}$  and  $OH^-$  ions that form water by protonation [30].

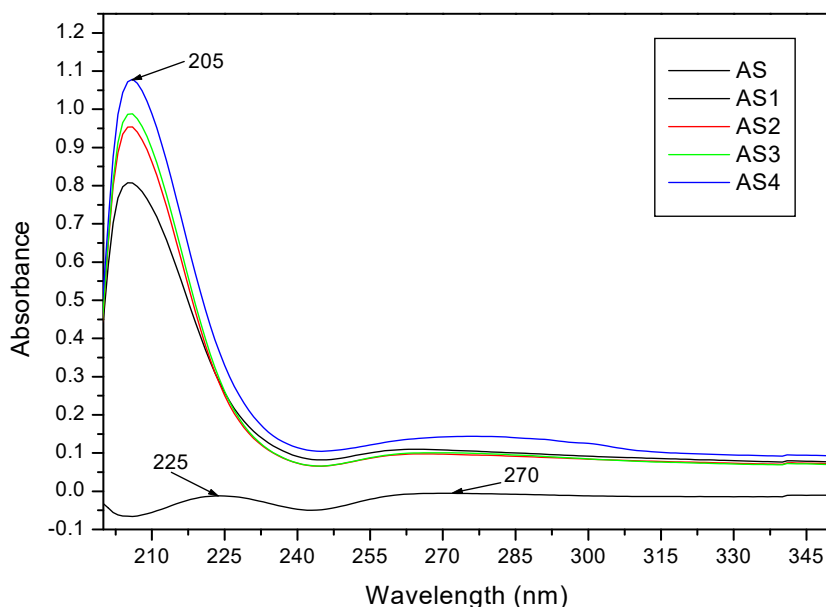


**Figure 5.** UV-VIS absorbance spectra of AS (as-prepared) and AS1, AS2, AS3 and AS4, which corresponds to AS after immersion of S1, S2, S3 and S4 composites, respectively.

One observation should be emphasized. Samples immersed in AS for 32 days did not form the HAP phase and this fact could favor the dissolution of the MgO phase. The release of biocompatible Mg<sup>2+</sup> ions acted as an inhibitor of HAP crystal growth suppressing unwanted crystallization *in vivo* [30].

In addition, the absorbance at 205 nm is increased with increasing MgO amount on the prepared composites. Further studies need to complete elucidate the *in vitro* complex mechanism which takes place.

## CONCLUSIONS

In order to improve the biological performances of the inert ZrO<sub>2</sub>, a different amount of antibacterial MgO and bioactive and biocompatible HAP, was added to ZrO<sub>2</sub> matrix. ZrO<sub>2</sub>-based biocomposites were successfully obtained by conventional ceramic method at 1550°C, followed by their characterization using XRPD, SEM and TEM techniques. The analyses indicated the presence of tetragonal ZrO<sub>2</sub> phase accompanied by periclase MgO with increasing its amount on the prepared biocomposites. HAP, or other CaP phases were not detected between the whole series of the prepared samples. Moreover, the stability and bioactivity of the prepared materials were tested by simulating the conditions from the oral cavity, by their immersion in artificial saliva (AS) for 32 days. The results suggest that MgO have an important role in the dissolution of biocomposites. Further studies need to understand both the physical and molecular level changes which take place following *in vitro* test of biocomposites.

## EXPERIMENTAL SECTION

### Preparation

#### *Preparation of HAP*

HAP was prepared by the precipitation method described in previous works [31-36] under continuous mechanical stirring. The following materials were used: 0.15 mol L<sup>-1</sup> solution of calcium nitrate tetrahydrate (Merck, Germany), 0.09 mol L<sup>-1</sup> solution of diammonium hydrogen phosphate (Merck), and 25 mass % ammonia solution (Posch Basic, Poland). The diammonium hydrogen phosphate and the ammonia solution were slowly added to the calcium nitrate solution. The pH of the reaction mixture was adjusted with ammonia solution to 11, and the reaction temperature was maintained at ambient temperature. The reaction mixture was stirred for 22 h. The Ca/P mole ratio was maintained at 1.67. After the reaction was accomplished, the precipitate was washed with ethanol and filtered. The filtered material was dried at 90 °C for 6 h.

### **Biocomposites preparation**

ZrO<sub>2</sub>-based bioceramics were obtained by ceramic processing route which involved mixing, compaction and sintering. Commercial pure ZrO<sub>2</sub> (Riedel-de Haën AG, Seelze, Germany, 99%, d<sub>50</sub>=22.842 μm), MgO (Alfa Aesar, Germany, 99.99%, d<sub>50</sub>=1.780 μm) and HAP powders (d<sub>50</sub>=0.015 μm) in different ratio were used as raw materials. The experimented compositions are presented in Table 2. The starting precursor powders were mechanically activated using an agate mortar and pestle. The resulted powders were mixed with 5% PVA and uniaxially cold pressed in a metallic dye into cylindrical pellets of 1 g with 10 mm in diameter at a pressure of 400 kgf using a Carver Inc. hydraulic press (Carver Inc, Wabash, IN, USA). Further, the pellets were sintered at 1550 °C under air atmosphere with a heating and cooling rate of 5 °C/min and dwell time of 12 h at the maximum temperature.

**Table 2.** The nominal composition (wt.%) and notation of the samples.

<b>Sample ID</b>	<b>ZrO<sub>2</sub> (wt.%)</b>	<b>MgO (wt.%)</b>	<b>HAP (wt.%)</b>
S1	94.75	5	0.25
S2	89.5	10	0.5
S3	84	15	1
S4	73.5	25	1.5

### **Dissolution analysis in AS**

In order to study the dissolution behavior of the heat treated biocomposites in physiological environment, the *in vitro* dissolution study was carried out by immersing the four different composites in artificial saliva (AS) for 32 days. The dissolution and the stability of the prepared pellets were assessed under static conditions in AS prepared by the following formulation [37]: 4200 mg/L NaHCO<sub>3</sub> (Merck, Germany), 500 mg/L NaCl (Reactivul, România), 200 mg/L KCl (Reactivul, România) and maintained at 37±0.1 °C by a Memmert incubator. Before the immersion the samples were sonicated for 10 min in acetone to be degreased and then rinsed with ultrapure water. One pellet of each composition was placed in a recipient with 100 mL of AS. The containers were removed from the incubator after 32 days and the solutions were further analyzed by UV-VIS spectroscopy. Finally, the pellets were removed from AS, were washed with ultrapure water and dried in oven at 100 °C for 24 h before XRPD, SEM and TEM analysis.

## Characterization Methods

### ***X-ray powder diffraction (XRPD)***

XRPD analysis was performed in order to investigate the structure of the samples using a Shimadzu XRD-6000 diffractometer operating at 40 kV, 30 mA with a monochromator of graphite for CuK $\alpha$  ( $\lambda=1.54060$  Å). The diffraction patterns were recorded in the  $2\theta$  range of 10–80 $^\circ$  at a scan speed of 2  $^\circ$ /min.

### ***Scanning Electron Microscopy (SEM)***

SEM analysis was performed using a Hitachi SU8230 (Tokyo, Japan) microscope. The electron microscope was coupled with an Aztec X-Max 1160 EDX detector (Oxford Instruments).

### ***Transmission Electron Microscopy (TEM)***

The size and shape of biocomposites crystallites were investigated by TEM on Hitachi H-7650 equipment.

### ***UV VIS spectroscopy***

Spectrophotometric measurements of AS before and after biocomposites' immersion were performed in 1 cm wide quartz cuvettes on a JASCO V-650 spectrophotometer.

## REFERENCES

1. K. Nakamura; T. Kanno; P. Milleding; U. Ortengren; *Int. J. Prosthodont.*, 2010, 23, 299-309
2. H. J. Wenz; J. Bartsch; S. Wolfart; M. Kern; *Int. J. Prosthodont.*, **2008**, 21, 27-36
3. M. Hisbergues; S. Vendeville; P. Vendeville; *J. Biomed. Mater. Res. B Appl. Biomater.*, **2009**, 88(2), 519-529
4. S. D. Heintze; V. Rousson; *Int. J. Prosthodont.*, **2010**, 23, 493-502
5. L. Nistor; M. Grădinaru; R. Rîcă; P. Mărășescu; M. Stan; H. Manolea; A. Ionescu; I. Moraru; *Curr. Health Sci. J.*, **2019**, 45, 28-35
6. J. S. Schley; N. Heussen; S. Reich; J. Fischer; K. Haselhuhn; S. Wolfart; *Eur. J. Oral Sci.*, **2010**, 118, 443-50
7. A. L. Gomes; J. Montero; *Med Oral Patol Oral Cir Bucal.*, **2011**, 16(1), e50-e55
8. A. J. Raigrodski; M. B. Hillstead; G. K. Meng; K.-H. Chung; *J. Prosthet Dent.*, **2012**, 107, 170-177
9. P. Triwatana; N. Nagaviroj; C. Tulapornchai; *J. Adv. Prosthodont.*, **2012**, 4, 76-83
10. E. D. Roumanas; *J. Evid. Based Dent. Pr.*, **2013**, 13, 14-5

11. R. D. L. Mattiello; T. M. K. Coelho; E. Insaurralde; A. A. K. Coelho; G. P. Terra; A. V. B. Kasuya; I. N. Favarão; L. de S. Goncalves; R. B. Fonseca; *ISRN Biomater*, **2013**, 1-10
12. R. H. French; S. J. Glass; F. S. Ohuchi; Y.-N. Xu; W. Y. Ching; *Phys. Rev. B.*, **1994**, *49*, 5133-5142
13. J. P. Goff, W. Hayes, S. Hull, M. T. Hutchings; K. N. Clausen; *Phys. Rev. B.*, **1999**, *59*(22), 14202-14219
14. I. Denry; J. R. Kelly; *Dent. Mater.*, **2008**, *24*, 3, 299-307
15. B. Al-Amleh; K. Lyons; M. Swain; *J. Oral Rehabil.*, **2010**, *37*, 641-52
16. J. Chevalier; L. Gremillard; A. V. Virkar; D. R. Clarke; *J. Am. Ceram. Soc.*, **2009**, *92*, 1901–20
17. E. C. Subbarao; Zirconia - an overview, in *Advanced Ceramics*, Science and Technology of Zirconia, A. H. Heurer and L. W. Hobbs Eds.; The American Chemical Society, Columbus, OH, USA, vol. 3, **1981**, pp.1-24
18. G. Wang; X. Liu; C. Ding; *Surf. Coatings Technol.*, **2008**, *202*, 5824-5831
19. Y.-W. Hsu; K.-H. Yang; K.-M. Chang; S.-W. Yeh; M.-C. Wang; *J. Alloys Compd.*, **2011**, *509*, 6864-6870
20. S. Nath; S. Baja; B. Basu; *Int. J. Appl. Ceram. Technol.*, **2008**, *5*(1), 49-62
21. Y. Rao; W. Wang; F. Tan; Y. Chi; J. Lu; X. Qiao; *Appl. Surf. Sci.*, **2013**, *284*, 726-731
22. K. Krishnamoorthy; G. Manivannan; S. J. Kim; K. Jeyasubramanian; M. Premanathan; *J. Nanopart. Res.*, **2012**, *14*(9), 1063, 1-10
23. S. Makhluif; R. Dror; Y. Nitzan; Y. Abramovich; R. Jelinek; A. Gedanken; *Adv. Funct. Mater.*, **2005**, *15*(10), 1708-1715
24. R. Z. LeGeros; *Clin. Orthop.*, **2002**, *395*, 81–98
25. I. Antoniac; *Bioceramics and Biocomposites: From Research to Clinical Practice*, Wiley-VCH, Weinheim, New York, **2019**, pp. 400
26. A. L. Patterson; *Phys. Rev.*, **1939**, *56*, 978-982
27. L. Renuka; H. P. Nagaswarupa; S. C. Prashantha; K. S. Anantharaju; S. C. Sharma; H. Nagabhushana; Y. S. Vidya; *J. Alloys Compd.*, **2016**, *672*, 609-622
28. L. Hu; C. Wang; Y. Huang; *J. Mater. Sci.*, **2010**, *45*, 3242–3246
29. B. Annaz; K. A. Hing; M. Kayser; T. Buckland; L. Di Silvio; *J. Microsc.*, **2004**, *215*, 100-110
30. L. Grima; M. Díaz-Pérez; J. Gil; D. Sola; J. I. Peña; *Appl. Sci.*, **2020**, *10*(1), 1-15
31. R. Barabás; M. Czikó; I. Dékány; L. Bizo; E. S. Bogya; *Chem. Pap.*, **2013**, *67*(11), 1414–1423
32. R. Barabás; E. de Souza Ávila; L. O. Ladeira; L. Mosqueira Antônio; R. Tötös; D. Simedru; L. Bizo; O. Cadar; *Arab. J. Sci. Eng.*, **2020**, *45*, 219-227
33. R. Barabás; D. Deemter; G. Katona; G. Batin; L. Barabas; L. Bizo; O. Cadar; *Turk. J. Chem.*, **2019**, *43*(3), 809-824
34. R. Barabás; N. Muntean; G. Szabó; K. Maurer; L. Bizo; *Studia UBB Chemia*, **2017**, *LXII*, 4(II), 253-268
35. E. S. Bogya, I. Bâldea, R. Barabás, A. Csavdári, G. Turdean, V. R. Dejeu, *Studia UBB Chemia*, **2010**, *2*(2), 363-373
36. R. Barabás, M. Rigó, M. Eniszné-Bódogh, C. Moisa, O. Cadar, *Studia UBB Chemia*, *LXIII*, **2018**, *3*, 137-154
37. K. Engelhart; A. Popescu; J. Bernhardt; *BMC Ear Nose Throat Disord.*, **2016**, *16*(6), 1-7